On the Structure of Polymeric Micelles: Self-Consistent-Field Theory and Universal Properties for Volume Fraction Profiles

F. A. M. Leermakers,* C. M. Wijmans,† and G. J. Fleer

Department of Physical and Colloid Chemistry, Wageningen Agricultural University, Dreijenplein 6, 6703 HB Wageningen, The Netherlands

Received October 31, 1994; Revised Manuscript Received January 30, 1995®

ABSTRACT: Polymeric micelles composed of asymmetric block copolymers of the type A_nB_m in a solvent S are analyzed by the self-consistent-field theory due to Scheutjens and Fleer. Micelle formation is studied in a spherical lattice geometry. An unfavorable mixing of A and S segments drives the self-assembly process, leading to micelles which can vary their aggregation number according to the conditions in solution. We study the micelle thermodynamics and the micelle structure as a function of the solvency of the B tails; the Flory–Huggins interaction parameter χ_{SB} has been varied from 0 (good solvent) to 0.5 (Θ solvent). With decreasing solvency the critical micelle volume fraction (CMV) decreases and the micelle size increases. The micelles have a dense core and a more dilute brushlike corona structure. Our main interest is in the density profiles of the corona. We distinguish four regimes in these profiles, denoted proximal, central, parabolic, and distal. The proximal part of the B profile is near the core and is nonuniversal, the central part is a power law which is in good agreement with the scaling predictions of Daoud and Cotton, in the third regime the profile of the polymer segments is roughly parabolic, and in the distal regime an exponential decay toward the bulk solution occurs. The relative importance of these regimes depends on the molecular architecture. For example, increasing the number of core (A) segments causes the central part first to grow and then to shrink in favor of the parabolic regime.

Introduction

Self-assembly of block copolymers into micelles receives increasing attention from the scientific community. Similar to their low molecular weight analogues, block copolymers exhibit a rich phase behavior.[1] There are, however, some interesting differences. For small surfactants the packing phenomena dominate, whereas in polymeric assemblies the chain statistics are more important. Therefore, one could expect a universal behavior for some of the properties of the polymeric systems. Second, in polymeric surfactants one can more rigorously vary the chemistry for tailor-made applications. At long enough sequences of two types of segments, these segments will show internal demixing and the typical surfactant functionality is automatically obtained. Small surfactants can, in favorable cases, be rather pure and monodisperse molecules. In contrast, polymeric surfactants are nearly always polydisperse, both in the A and in the B block. This has important consequences for the critical micelle concentration and the composition of the micelles.[2]

In this paper we will, however, assume that the copolymers are monodisperse. We will focus on spherical aggregates of asymmetric polymeric surfactants formed in a selective solvent, restrict ourselves to the dilute micellar solutions so that the micelles do not interact, and consider all micelles to be of the same size, thereby neglecting size and shape polydispersity of the aggregates. The insoluble block of A segments is relatively short and is repelled from the solution phase, which is modeled as monomeric components S. This unfavorable mixing drives the micelle formation, and a rather compact dense core is formed. A much larger soluble block of B segments makes up a buoy layer of protruding tails. This brush forms a protective layer around the core and is often called the corona.[3–5] The chain parts of most of the corona are highly stretched due to an excluded-volume potential. The free energy cost of stretching of the brush chains opposes the mixing energy gain by the A segments. In equilibrium these two effects balance each other and this balance determines the aggregation number.

Polymer brushes, such as those found in the corona of polymeric micelles, can be modeled in several ways. The recognition by Semenov that in the case of strongly stretched chains it is allowed to replace the full set of explicit conformations by an "average trajectory"[6] triggered many investigations. Independent from each other Milner, Witten, and Cates[7] and Zhulina, Borisov, and Priamitsyn[8] elaborated this idea for polymer grafted on a solid surface and derived approximate analytical solutions. A recent analysis of Wijmans and Zhulina,[9] who compared analytical and numerical approaches of curved polymer brushes, motivated us to investigate the structure of the corona of spherical micelles. For an end-grafted polymer brush on a spherical particle two regimes are distinguished in the polymer layer: (i) a power-law part in the region with high curvature (near the surface) and (ii) a parabolic potential profile at the periphery of the brush where the curvature is much less. For the power-law part of the profile we may write:

$$\begin{cases} \varphi(z) \propto z^{-1} & \Theta \text{ solvent} \\ \varphi(z) \propto z^{-4/3} & \text{good solvent} \end{cases} \quad (1)$$

where z is the distance to the center of the particle and φ is the volume fraction of the polymer units. The scaling relations of eq 1 coincide with the well-known results of Daoud and Cotton[10] for star-shaped polymers. The power-law piece of the profile is part of the so-called "dead zone". This dead zone is a region in the density profile (next to the particle surface), which contains no tail ends. The dead zone is not restricted to the power-law regime (i) but also extends slightly into the parabolic regime (ii). In the outer parts of the spherical brush layer, the curvature is reduced to such an extent that the profile gradually returns to the profiles that correspond to the well-known parabolic potential profiles for flat brushes. The numerical calculations of Wijmans

† Present address: Physical Chemistry 1, Chemical Center, University of Lund, P.O. Box 124, S-221 00 Lund, Sweden.

® Abstract published in *Advance ACS Abstracts,* March 15, 1995.

0024-9297/95/2228-3434$09.00/0

and Zhulina agree reasonably well with the expected scaling relationship and are consistent with a similar analysis of Milner and Witten.[11]

Over the past years a large number of papers have been published on systems with end-tethered polymers. Besides the analytical and numerical self-consistent-field modeling and the scaling approach mentioned above, computer simulations techniques have been used to model these systems.[12] Some of these papers were motivated by the expectation that insights obtained for grafted layers can be applied to polymeric micelles. However, there are relatively few complete analyses of the complicated problem of self-assembly.[1,3,13-16] In a full analysis one should take into account that the number of chains in a micelle adjusts itself to a variation of the polymer (and micelle) concentration.[14] In such an analysis it is important that the thermodynamic criteria for equilibrium and stability are obeyed.[17] In simulation techniques accurate evaluation of thermodynamic quantities is virtually impossible, which makes these methods unsuitable for studying polymeric micellar equilibria. On the other hand, analytical approaches for self-assembling systems need many drastic assumptions as to the structure of the micelles.

We make use of the numerical self-consistent-field (SCF) approach for chain molecules in inhomogeneous systems due to Scheutjens and Fleer.[18-21] The application of this theory to micellar systems was developed by Leermakers *et al.*[22-27] for surfactant systems and first applied to polymeric micelles by Van Lent *et al.*[28] Recently, others used this approach for the modeling of poly(ethylene oxide)–poly(propylene oxide) (PEO–PPO) nonionic systems.[2,15,16,29] The molecules in a SCF modeling are allowed to distribute themselves freely throughout the system. This complexity does not prevent one from calculating accurate thermodynamic quantities needed for the equilibrium and stability analysis.

In the following we will summarize the fundamental aspects of the thermodynamics of micellar solutions and discuss the basics of the SCF theory. In the Results section we will focus on the corona structure of asymmetric block copolymers in selective solvents.

Statistical Thermodynamics of Micelle Formation

For a solution of free copolymer chains and copolymer aggregates we may write:

$$\mathrm{d}U = T\,\mathrm{d}S - p\,\mathrm{d}V + \sum_i \mu_i\,\mathrm{d}n_i + \epsilon\,\mathrm{d}n_\mathrm{m} \qquad (2)$$

The extensive properties are the energy U, the entropy S, the volume V, the number n_i of molecules of component i (in this case solvent and copolymer), and the number of micelles n_m. The intensive quantities are the temperature T, the pressure p, the chemical potentials μ_i of component i, and the intensive conjugate ϵ of the number of micelles. The latter quantity can be identified as the excess chemical potential of a micelle and should include all (free) energy quantities that scale with n_m and which are not yet included in the chemical potentials. In the nomenclature of Hall and Pethica,[17] n_m is the number of small systems and ϵ is the subdivision potential.

For a closed isothermal system it is convenient to define the Gibbs free energy as $G = U + pV - TS$. Then the usual Legendre transform gives

$$\mathrm{d}G = -S\,\mathrm{d}T + V\,\mathrm{d}p + \sum_i \mu_i\,\mathrm{d}n_i + \epsilon\,\mathrm{d}n_\mathrm{m} \qquad (3)$$

From eq 3 we obtain the equilibrium condition

$$\left(\frac{\partial G}{\partial n_\mathrm{m}}\right)_{T,p,\{n_i\}} = \epsilon = 0 \qquad (4a)$$

and the stability criterion

$$\left(\frac{\partial \epsilon}{\partial n_\mathrm{m}}\right)_{T,p,\{n_i\}} > 0 \qquad (4b)$$

Equation 4a expresses that there is no extra free energy associated with the formation of a micelle: the free energy G is fully determined by the chemical potentials of the molecules in the system. This is consistent with a mass action model, which can be seen as follows. We return to eq 3 and choose conditions of constant p and T. The Gibbs free energy G reads $\mathrm{d}G = \sum_i \mu_i\,\mathrm{d}n_i + \epsilon\,\mathrm{d}n_\mathrm{m}$. We now divide the molecules in the system into two classes: those in solution are indicated by a superscript s and those associated in the micelles by the superscript m. For the chemical potentials the superscript can be omitted since $\mu_i^\mathrm{m} = \mu_i^\mathrm{s} = \mu_i$. We can now define the chemical potential of a micelle as:

$$\hat{\mu} = \sum_i \mu_i \bar{n}_i^\mathrm{m} + \epsilon \qquad (5)$$

where $\bar{n}_i^\mathrm{m} = n_i^\mathrm{m}/n_\mathrm{m}$ is the average number of molecules of type i in a micelle. We may write:

$$\mathrm{d}G = \sum_i \mu_i\,\mathrm{d}n_i^\mathrm{s} + \hat{\mu}\,\mathrm{d}n_\mathrm{m} \qquad (6)$$

Upon integration we now find for the total free energy:

$$G = \sum_i \mu_i^\mathrm{s} n_i^\mathrm{s} + \hat{\mu} n_\mathrm{m} \qquad (7)$$

In this approach, the micelle is considered as an extra component in the system and all molecules associated in micelles are extracted from the solution. The mass action model[30] defines the equilibrium by $\hat{\mu} = \sum_i \mu_i \bar{n}_i^\mathrm{m}$. Hence the mass action model dictates that in eq 5 $\epsilon = 0$, which is consistent with eq 4a.

The application of eq 4 in a statistical thermodynamical model is not trivial. A detailed molecular model is needed to systematically compute the subdivision potential. By doing so, one can select those aggregates for which the equilibrium constraint (eq 4a) and the stability constraint (eq 4b) are obeyed. Exact computations are not yet possible, and an approximate model must be used. In an SCF model we can compute the subdivision potential as follows. We can write for the chemical potential of the micelles in dilute solutions:

$$\hat{\mu} = k_\mathrm{B}T \ln \varphi_\mathrm{m} + \sum_i \bar{n}_i^\mathrm{m} \mu_i + \mathrm{A}^\sigma \qquad (8)$$

where k_B is the Boltzmann constant and φ_m is the volume fraction of micelles. In eq 8 the first term on the right-hand side accounts for the translational entropy of a micelle as a whole, the second term has been discussed above, and the third one is the translationally restricted excess free energy of the micelle. The second and third term form together the free energy of

the micelle of which the translational entropy is excluded. Such a micelle is modeled in the SCF calculations. By comparison with eq 5 we find that the volume fraction of micelles is directly coupled to the translationally restricted excess free energy of the system:

$$\varphi_m = e^{-A^\sigma/k_BT} \tag{9}$$

since $\epsilon = 0$. The excess free energy of a small system wherein we have immobilized a micelle is computed in our model by fixing the micelle to the center of a spherical lattice. For such a system we can evaluate the radial segment distributions and obtain from these the excess free energy $A^\sigma = G - \sum_i \bar{n}_i\, d\mu_i$ as[21]

$$\frac{A^\sigma}{k_BT} = \sum_z L(z)\left[-\sum_i \frac{\varphi_i(z) - \varphi_i^b}{N_i} + \sum_A \varphi_A(z) \ln G_A(z)\right] + \sum_z L(z)\left[\frac{1}{2}\sum_A\sum_B \chi_{AB}\{\varphi_A(z)\,(\langle\varphi_B(z)\rangle - \varphi_B^b) - \varphi_A^b(\varphi_B(z) - \varphi_B^b)\}\right] \tag{10}$$

where $L(z)$ is the number of lattice sites in layer z, $\varphi_i(z)$ and φ_i^b are the volume fractions of component i in layer z and the bulk solution, respectively, $\varphi_A(z)$ and φ_A^b are the contributions due to segment type A, χ_{AB} is the usual Flory–Huggins interaction parameter between segment types A and B, and N_i is the number of segments in a molecule of type i. The angular brackets denote an average over three layers; compare eq 21. Finally, the segmental weighting factor $G_A(z)$ is defined as $G_A(z) = \exp(-u_A(z)/k_BT)$, where the potential $u_A(z)$ is given by eq 19.

The chemical potentials are evaluated in our SCF method by the Flory–Huggins equations, generalized to an arbitrary number of components in the system:[21]

$$(\mu_i - \mu_i^*)/k_BT = \ln \varphi_i^b + 1 - N_i\sum_j \frac{\varphi_j^b}{N_j} + \frac{N_i}{2}\sum_A\sum_B \chi_{AB}(\varphi_{Ai}^* - \varphi_A^b)(\varphi_B^b - \varphi_{Bi}^*) \tag{11}$$

where the asterisk refers to the pure amorphous phase which serves as the reference system. The quantity φ_{Ai}^* is the volume fraction of segments A in the pure amorphous component i, which equals the fraction of A segments in the chain. As before, the superscript b refers to the bulk of the solution, that is to the part of the system outside the micelles, where no concentration gradients exist.

From eq 9 we learn that A^σ cannot be negative. Additional information is obtained by analyzing the stability constraint as given by eq 4b. From eqs 5 and 8 it follows that $\epsilon = A^\sigma + k_BT \ln \varphi_m$. Hence,

$$\left(\frac{\partial\epsilon}{\partial n_m}\right)_{T,p,\{n_i\}} = \left(\frac{\partial[A^\sigma + k_BT \ln \varphi_m]}{\partial n_m}\right)_{T,p,\{n_i\}} \approx \left(\frac{\partial A^\sigma}{\partial \bar{n}_p^\sigma}\frac{\partial \bar{n}_p^\sigma}{\partial n_m}\right)_{T,p,\{n_i\}} > 0 \tag{12}$$

In eq 12 we have neglected $\partial \ln \varphi_m/\partial n_m = (1/\varphi_m)\,\partial\varphi_m/\partial n_m = n_m^{-1}$, which is extremely small in a macroscopic system. Let $\bar{n}_p^\sigma = \sum_z L(z)\,(\varphi_p(z) - \varphi_p^b)/N_p$ be the excess number of copolymer molecules in a micelle (the summation over z extends over the volume of the small system); then the mass balance equation for the copolymers in the entire solution (containing n_m micelles) can be written as:

$$n_p = \bar{n}_p^\sigma n_m + \varphi_p^b V/N_p \tag{13}$$

From eq 13 it follows that $\partial\bar{n}_p^\sigma/\partial n_m = -\bar{n}_p^\sigma - (V/N_p)\,\partial\varphi_p^b/\partial n_m$ where V is the volume of the whole system. In general, $\bar{n}_p^\sigma$ is a positive quantity but $\phi\varphi_p^b/\partial n_m$ is negative, and it is not trivial to unambiguously determine the sign of $\partial\bar{n}_p^\sigma/\partial n_m$. In the limit that almost all the polymer is associated into micelles (well above the critical micelle volume fraction (CMV)) we have $n_p \approx \bar{n}_p^\sigma n_m$ and thus $\partial\bar{n}_p^\sigma/\partial n_m < 0$. In the other limit, where almost all the polymer is *not* associated, we have $n_p \approx \varphi_p^b V/N_p$ and thus $\partial\varphi_p^b/\partial n_m \approx 0$. This leads also to $\partial\bar{n}_p^\sigma/\partial n_m < 0$. Moreover, it is very unlikely that $\partial\bar{n}_p^\sigma/\partial n_m = 0$. This can, in principle, only occur when all the surfactants used to form a new micelle are taken from the bulk solution. In this case $\bar{n}_p^\sigma = -V/N_p\,\partial\varphi_p^b/\partial n_m$. It can be shown that the condition $\partial\bar{n}_p^\sigma/\partial n_m > 0$ would imply that $\partial\mu_p/\partial\varphi_p^b < 0$, which is obviously impossible. Consequently, the derivative $\partial A^\sigma/\partial\bar{n}_p^\sigma$ must be negative to have macroscopically stable micelles (cf. eq 12). The numerical analysis of the free energy as a function of the micelle size is in line with this stability criterion.

In our calculations we can generate micelles that are not necessarily macroscopically stable because we enforce one *single* micelle in one *small* system; however, the thermodynamically stable micelles can be selected by using $A^\sigma = -k_BT \ln \varphi_m$ ($A^\sigma > 0$) and $\partial A^\sigma/\partial\bar{n}_p^\sigma < 0$.

SCF Model

From the equations given above it is clear that information on the segment density throughout a small system is sufficient to evaluate all the thermodynamic parameters. In the SCF theory these distributions are obtained using a number of approximations.[21] An important step in the theory is to discretize space by using a lattice with spherical layers. We apply a mean-field approximation in each layer. The segment density is assumed to be constant throughout the layer. Layers are numbered from the central layer outward: $z = 1, \ldots, M$, where M is a layer far removed from the center. The number of lattice sites per layer is given by $L(z) = (4/3)\pi(z^3 - (z-1)^3)$; for large z, $L(z)$ increases quadratically with z. Molecules are composed of segments with ranking number $s = 1, \ldots, N_i$, where N_i is the chain length of molecule i. The molecules may be composed of various segment types: A for the apolar segments, B for the soluble (buoy) segments, and S for the solvent. Usually (but not necessarily), a solvent molecule contains one segment S. The segment distribution of a given segment s of molecule i is given by $\{\varphi_i(z,s)\}$. Defining $\delta_{i,s}^A$ as being unity when segment s of molecule i is of type A and zero otherwise, we may write

$$\varphi_A(z) = \sum_i\sum_s \varphi_i(z,s)\,\delta_{i,s}^A \tag{14}$$

which gives the overall segment density of segment type A irrespective of the molecule or the ranking number. Conjugated to the $\varphi_A(z)$ profile we define a segmental potential profile $u_A(z)$. Correlations due to the con-

nectivity of segments are accounted for by using a first-order Markov approximation. From the point of view of the chain statistics $u_A(z)$ may be considered as an external potential which weights the otherwise random walks of the chains. We define the Boltzmann factor $G_A(z) = \exp(-u_A(z)/k_BT)$ as a free segment distribution function. The Markov approximation allows the computation of the segment densities by a composition law connecting two step-weighted random walks:

$$\varphi_i(z,s) = C_i G_i(z,s|1)\, G_i(z,s|N)/G_i(z,s) \qquad (15)$$

where $G_i(z,s|1)$ and $G_i(z,s|N)$ are chain-end distribution functions which collect the statistical weight of all conformations of subchains from segment 1 to s and N to s, respectively. These distributions can be found by a propagator method. The quantity $G_i(z,s)$ is the free segment distribution function for segment s of component i; it equals $G_A(z)$ if segment s is of type A or, mathematically, $G_i(z,s) = \sum_A \delta_{i,s}{}^A G_A(z)$, where the summation over A is over all segment types A = A, B, S. The chain-end distribution functions are related to the end distribution of chains that are one segment shorter:

$$G_i(z,s|1) = G_i(z,s) \sum_{z'=z-1,z,z+1} \lambda(z|z')\, G_i(z',s-1|1) = G_i(z,s)\, \langle G_i(z,s-1|1)\rangle$$

$$G_i(z,s|N) = G_i(z,s) \sum_{z'=z-1,z,z+1} \lambda(z|z')\, G_i(z',s+1|N) = G_i(z,s)\, \langle G_i(z,s+1|N)\rangle \qquad (16)$$

The angular brackets denote an average over three layers. In eq 16 $\lambda(z|z')$ is the *a priori* step probability going from a layer z' to z. Obviously, $\lambda(z|z) = 1 - \lambda(z,z-1) - \lambda(z|z+1)$ for all z. Given that $A_s(z) = 4\pi z^2$ is the surface between the layers z and $z+1$, we can write:

$$\lambda(z|z-1) = \frac{1}{3}\frac{A_s(z-1)}{L(z)}$$

$$\lambda(z|z+1) = \frac{1}{3}\frac{A_s(z)}{L(z)} \qquad (17)$$

where the normalization $^1/_3$ is chosen because this choice can be shown to minimize so-called lattice artifacts. Equation 16 can be performed iteratively, until the free chain ends are reached, where $G_i(z,1|1) = G_i(z,1)$ and $G_i(z,N|N) = G_i(z,N)$. The normalization constant C_i of eq 15 is the only quantity which still needs to be defined. In the calculation we fix the total number $\bar{n}_i$ of molecules of type i in the small system: $\bar{n}_i = N_i{}^{-1}\sum_z \sum_{s=1}{}^{N_i} L(z)\, \varphi_i(z,s)$. Hence,

$$C_i = \frac{\bar{n}_i}{\sum_z L(z)\, G_i(z,1|N)} \qquad (18)$$

From C_i we can obtain the volume fraction of component i in the bulk as $\varphi_i{}^b = C_i N_i$.

The segment potential $u_A(z)$ for segments of type A in layer z is assumed to be composed of two contributions:

$$u_A(z) = u'(z) + k_BT \sum_B \chi_{AB}\Big[\sum_{z'=z-1,z,z+1} (\lambda(z|z')\, \varphi_B(z')) - \varphi_B{}^b\Big] = u'(z) + k_BT \sum_B \chi_{AB}[\langle \varphi_B(z)\rangle - \varphi_B{}^b] \qquad (19)$$

The first term $u'(z)$ is a Lagrange parameter which follows from the constraint that each layer is exactly filled or, in other words, that each lattice site is on average filled exactly once:

$$\sum_A \varphi_A(z) = 1 \qquad \forall z \qquad (20)$$

The second term in eq 19 is the usual expression which accounts for the various contacts of segments of type A in layer z, according to a Bragg–Williams approximation. The summation A runs over all segment types in the system (A = A, B, S). The quantity within the angular brackets is often called the site fraction, for which in a spherical symmetry one can write:

$$\langle \varphi(z)\rangle \approx \varphi(z) - \frac{1}{3}\frac{2}{z}\frac{\partial \varphi(z)}{\partial z} + \frac{1}{3}\frac{\partial^2 \varphi(z)}{\partial z^2} \qquad (21)$$

For interfacial problems it is well-known that the second derivative of the density profile with respect to z in $u_A(z)$ (the third term in eq 21) is essential to obtain reliable results. The first derivative (second term in eq 21) accounts for the spherical geometry and vanishes for large z.

The above set of equations is closed, and a fixed point, also called the self-consistent solution, is found numerically without any additional assumptions. Numerical details can be found elsewhere.[31]

Results

Parameters. For most computations we have employed block copolymers $A_{50}B_{500}$, dissolved in a solvent S. We vary the solvency parameter χ_{BS} for the B units, but we fixed the interaction parameters for the segments A: $\chi_{AB} = 0.5$ and $\chi_{AS} = 2$. The latter value is high enough to give a strong driving force for phase separation of the A and S segments. We also choose a moderate repelling force between A and B segments. Note that the A and S segments repel each other more strongly than the A and B segments. The difference is large enough to expect that the B segments, rather than the solvent, adsorb onto the core (consisting of units of A). In systems that are characterized by steep gradients in the segment density profile, such as they occur in the core–corona interface, the problem of lattice artifacts is notorious. These artifacts show up as oscillations (with a period of a lattice layer) of the excess free energy and of the chemical potentials, as the interface is moved over the lattice.[14] The latter oscillations are out of phase compared to the former ones. The amplitude of the oscillations depends on the lattice type used, being large for a cubic lattice and much smaller for a hexagonal one. The smallest errors were found for a lattice where $\lambda(z|z) = \lambda(z|z-1) = \lambda(z|z+1) = {}^1/_3$ for large z. Calculations were performed for a small system composed of M = 200 layers. At the periphery (i.e., at z = 200), reflecting boundary conditions were chosen: $\varphi_A(201) = \varphi_A(200)$ and $u_A(201) = u_A(200)$ for all segment types A.

Thermodynamics. For a given calculation we fix the number of copolymer molecules and the number of

Table 1. Collection of Relevant Thermodynamic Data at the CMV for the Systems Given in Figure 1: the Critical Micelle Volume Fraction (CMV), the Chemical Potential of the Polymer, the Aggregation Number in the Micelle, and the Dimensionless Excess Free Energy of the Micelle

	$\chi_{BS} = 0$	$\chi_{BS} = 0.1$	$\chi_{BS} = 0.2$	$\chi_{BS} = 0.3$	$\chi_{BS} = 0.4$	$\chi_{BS} = 0.5$
CMV	3.4×10^{-14}	1.1×10^{-14}	3.0×10^{-15}	5.7×10^{-16}	5.7×10^{-17}	1.3×10^{-18}
$[(\mu_p - \mu_p^*)/k_BT](CMV)$	−502.7	−453.8	−405.2	−356.8	−309.1	−262.3
$n_p(CMV)$	14.5	16.8	20	24	32	54
$A^\sigma(CMV)/k_BT$	38.6	42.5	47.1	53.9	65.6	94.1

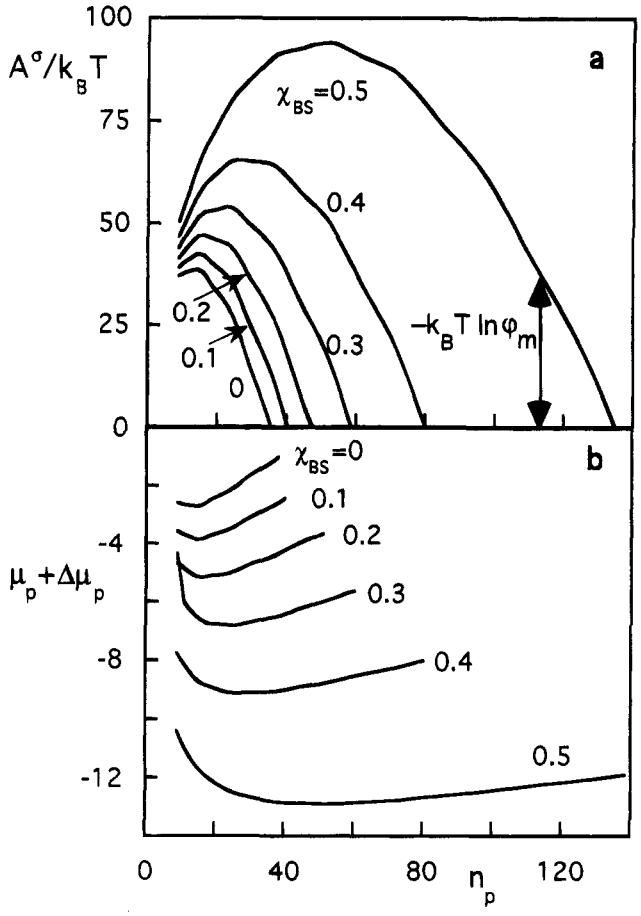

Figure 1. (a) Excess free energy of a translationally restricted polymeric micelle composed of $A_{50}B_{500}$ polymeric surfactants. (b) Chemical potential ($(\mu_p - \mu_p^*)/k_BT$ is abbreviated as μ_p) of the $A_{50}B_{500}$ molecules as a function of the aggregation number (we have used the notation n_p replacing $\bar{n}_p^\sigma$). The interaction parameter for the B segments with the solvent is indicated. $\Delta\mu_p$ is an arbitrary offset which was chosen as 500, 450, 400, 350, 300, and 250 for χ_{BS} = 0, 0.1, 0.2, 0.3, 0.4, and 0.5, respectively.

solvent molecules in the 200-layer system. The SCF solution has one micelle in the center of the lattice, and all density profiles converge to the constant bulk value going out toward layer M. The system is in its free energy minimum, given the constraint of one micelle in the center of the small system. Without analyzing the thermodynamics of a micellar system, one cannot say anything definite on the macroscopic stability of such a micelle. In Figure 1 we show the thermodynamic data of a series of calculations where we have varied the number of copolymers in the small system. (Note that from here on we use n_p for $\bar{n}_p^\sigma$ because we will discuss the properties of the small systems only. Further, the polymer concentration in the bulk is very low, and we can ignore, in the numerical data, the difference between n_p^σ and n_p.) In addition we have systematically varied the solvency parameter from a good solvent to Θ conditions for the units that form the corona: χ_{BS} is varied from 0 to 0.5.

In Figure 1a, the thermodynamically stable region of the micellar system is the region to the right of the maximum in A^σ (Figure 1a) or in the minimum in μ_p (Figure 1b). The extra constraint is that A^σ should remain positive.

Each point on this stable branch of $A^\sigma(n_p)$ in Figure 1a corresponds to a micellar concentration $\varphi_m = \exp(-A^\sigma/k_BT)$ according to eq 9. The lowest possible micelle concentration corresponds with the highest possible A^σ; hence, the maximum in A^σ corresponds to the critical micelle volume fraction (CMV). The maximum in Figure 1a is found at the same aggregation number as the minimum in Figure 1b. This can be shown as follows. By taking the ratio of the slopes in parts a and b of Figure 1, we find $(\partial A^\sigma/\partial n_p)/(\partial\mu_p/\partial n_p) = \partial A^\sigma/\partial\mu_p$. This last ratio is, according to Gibbs' law, equal to minus the polymer aggregation number. The number of copolymer molecules in the micelle is a positive quantity for all micelle sizes so that the slopes in parts a and b of Figure 1 must have opposite signs and that the maximum in Figure 1a must coincide with the minimum in Figure 1b.

To the right of the maximum in A^σ and the minimum in μ_p, the decrease of A^σ is stronger than the increase of μ_p. Hence, $-(\partial A^\sigma/\partial\mu_p) = n_p$ increases (as indicated along the abscissa) and n_p increases with increasing micellar concentration φ_m. The lowest values of n_p and φ_m are found at the CMV. At the CMV both $\partial A^\sigma/\partial n_p$ and $\partial\mu_p/\partial n_p$ are zero. A physical interpretation of the ill-defined ratio of slopes at the maximum and minimum points in parts a and b of Figure 1, respectively, reflects the fact that the critical micelle volume fraction (CMV) is exactly at this point. Just below this concentration the micelle size is zero, which abruptly changes to micelles of finite size just above the CMV, as could be expected for a first-order phase transition. In other words, at the CMV the fluctuations in micelle size are very large. In our calculations we compute, for a given composition, a given micelle size and ignore fluctuations of this quantity. We only indirectly obtain information about the fluctuations from the thermodynamical analysis. Table 1 collects some relevant data of the six systems presented in Figure 1. For polymeric surfactants under the present conditions the theoretical CMV is far too low to be measured experimentally. One can alternatively suggest to define the CMV as the point where the concentration of micelles equals the concentration of free surfactants. For copolymers this concentration can still be very low which makes this choice not always practical. In experiments the first notion of micelles often occurs when the micelle concentration exceeds a threshold value. We thus may define an ad hoc "CMV" to be found at a given A^σ value, or equivalently at a given micelle concentration (cf. eq 9).

The small oscillations in the curves are due to lattice artifacts, but they do not seriously hinder our interpretations. These oscillations are much larger in other lattice types; see, e.g., ref 14.

It follows from eq 9 that at the CMV the micelle concentration φ_m is not arbitrarily low but has a finite

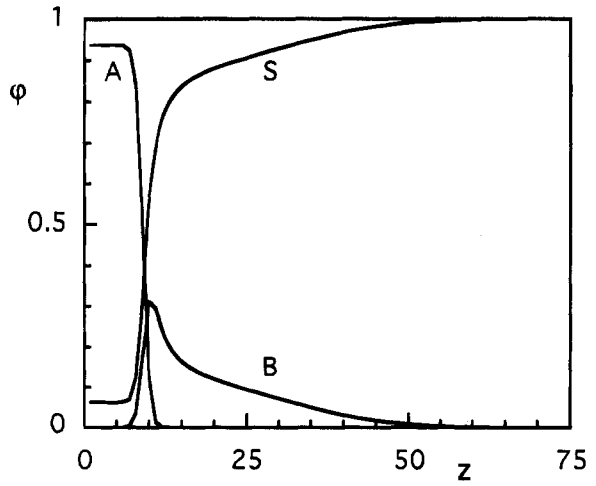

Figure 2. Radial volume fraction profile through a spherical micelle of $A_{50}B_{500}$ molecules. Parameters: $\chi_{BS} = 0.5$, $n_pN_p = 28\,000$.

value given by $\exp(-A^\sigma(\mathrm{CMV})/k_BT)$. For all points on the curves given in Figure 1 which obey the stability conditions, we can define a micellar system with a given micelle concentration. As at each of these points the micelle size and the chemical potentials are available, we can calculate the overall composition of the system. Clearly, the lower A^σ, the higher the micellar concentration φ_m and the overall polymer concentration in the system. We also learn from Figure 1a that the micelle size increases when A^σ decreases and thus that the micelles grow with increasing micelle concentration. Only small changes in the micelle size are expected with increasing surfactant concentration if the $A^\sigma(n_p)$ curve is steep. With increasing χ_{BS} we observe the $A^\sigma(n_p)$ curve to become less steep. This indicates that micelles for which the B block is in poorer solvent can increase their size more easily than micelles with the B block in a good solvent.

Finally, we note that one should be careful to interpret the $A^\sigma(n_p)$ curves for the regime where A^σ is of order unity. Then the micelle concentration is very high and micelle–micelle interactions are present. It has also been shown that, when the excess free energy per aggregate becomes very small, shape fluctuations are increasingly important.[25] Then the assumption of spherical micelles usually breaks down.

Segment Density Profiles. An example of the radial segment density distribution in a micelle is given in Figure 2. This example is for a polymer with a length of $N_p = 550$ ($A_{50}B_{500}$) in a Θ solvent for B units. In the micelle in total 28 000 polymer segments are aggregated ($n_p = 28000/550 \approx 51$). We notice from Figure 2 that in the dense core a small but finite amount of solvent (S) is absorbed. The interface between the A-rich core and the corona region which is rich in S is relatively sharp because of the high value of χ_{AS}. The B segments in the corona form a spherical brush which extends over many layers and is much richer in solvent than the core. The A segments are nearly completely depleted from

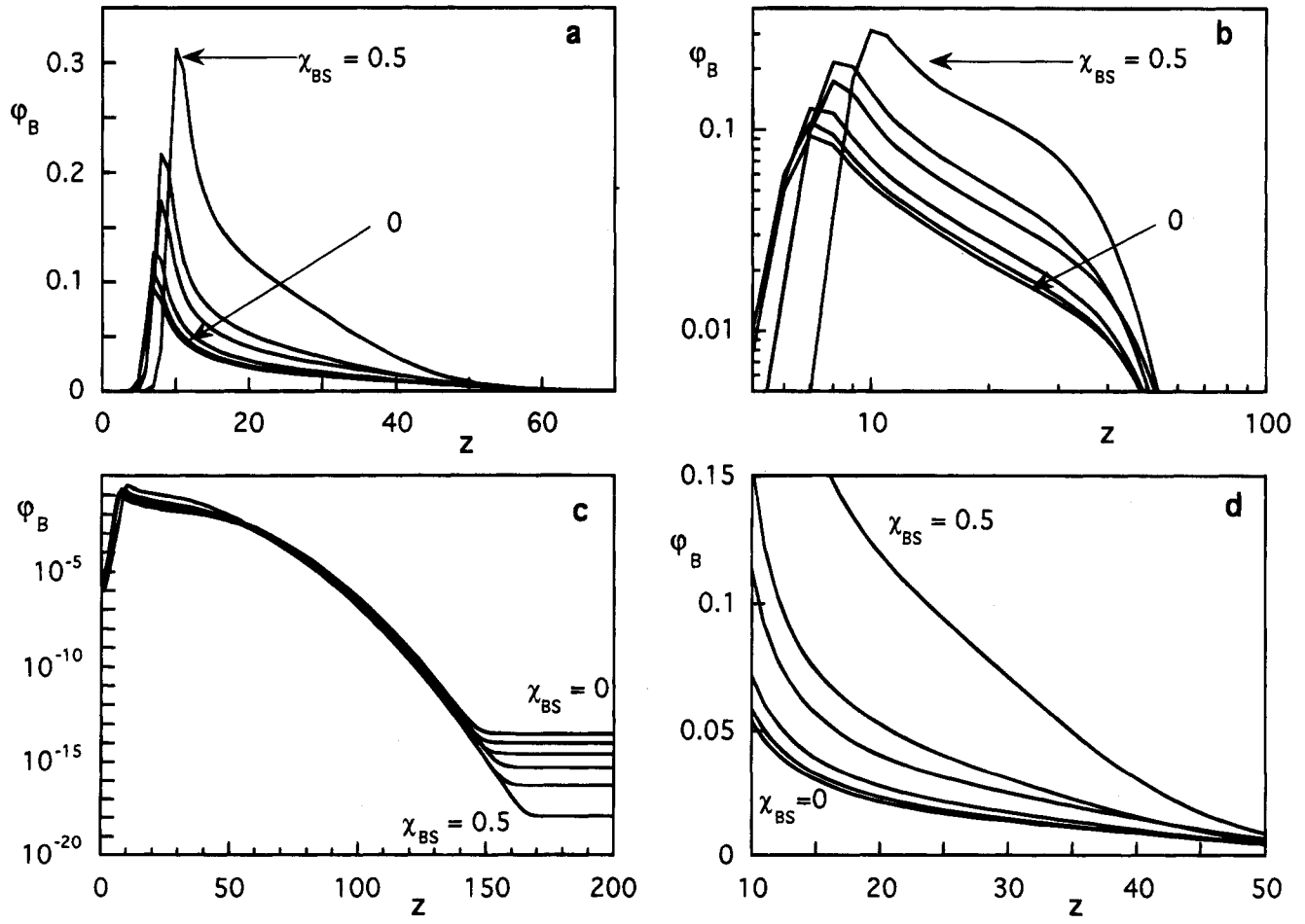

Figure 3. Radial volume fraction profiles for the B block of the micelles presented in Figure 1 at the CMV. The χ_{BS} parameters are 0, 0.1, 0.2, 0.3, 0.4, and 0.5. The relevant thermodynamic data are collected in Table 1. In diagram a we have plotted the profiles on a linear–linear scale, in b on a log–log scale, in c on a log–linear scale, and in d again on a linear–linear scale but in a narrower region than in a.

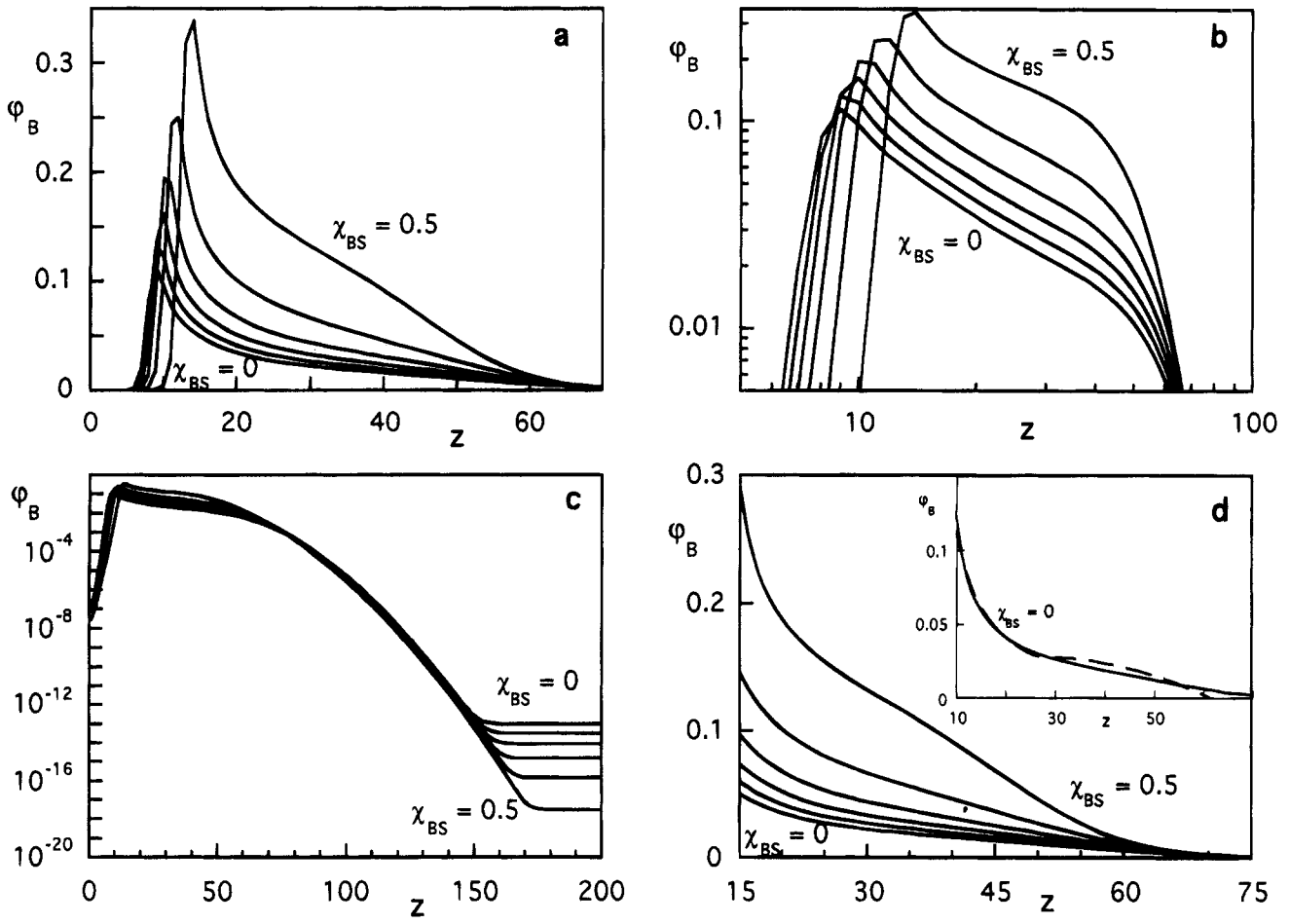

Figure 4. Segment density profiles for micelles of which the thermodynamics is given in Figure 1, at an excess free energy of 10 kT. In the inset of panel d the curve for $\chi_{BS} = 0$ is replotted together with the predictions made by the analytical theory of Wijmans and Zhulina[9] (dashed curve).

this region, as are the B segments from the core. The maximum of the B profile is positioned at the edge of the core. This is expected because the B units are in effect tethered onto the core. The density of B units next to the core is, however, higher than expected from a grafting condition. This is due to the adsorption of the B segments onto the core. With the present set of interaction parameters the B segments repel the A units, but the repulsion between the A and S units is stronger than that between the A and B units. Thus, there is still an energetic driving force for adsorption of the B units onto the surface of the core.

In the following figures we examine the brush profile in more detail. We do not show the core segments in the following graphs but note that the position of the maximum in the B profile is a good measure for the size of the core.

In Figures 3–5 the brush profiles of the six systems (Figure 1) are analyzed in detail. There are several ways to compare the systems. We choose the following approach. In Figure 3 we present the profiles for the systems at the theoretical CMV (thus at the maximum of Figure 1a); in Figure 4 we compare systems with a given excess free energy. A third way to present the data is given in Figure 5, where micellar systems at a given aggregation number are compared. The profiles are presented in various ways (linear–linear, log–linear, log–log) in order to recognize all the relevant profile information.

It is perhaps most instructive to start the discussion with the log φ versus log z plot in Figure 3b. Beyond the maximum, there appears to be a power-law regime in the density profile, which extends over some 20–30 layers. We might call this part the *central* part of the profile. The term central is used because of the analogy with the polymer adsorption profile as discussed by de Gennes.[32] Note, however, that in polymer adsorption the occurrence of a central part in the profile has a different physical origin. Toward the core side of this central part we notice upward deviations from the power law. This is due to the adsorption of B segments onto the core; this part of the profile might be called *proximal*, again after de Gennes.[32] The downward deviations in Figures 3b and 4b on the solution side of the central regime signal the onset of a *parabola-like* profile. A similar region was found by Wijmans and Zhulina for polymer grafted on small particles.[9]

The exponent in the central regime shows excellent correspondence with theoretical predictions. For all χ_{BS} values other than 0.5 we observe rather accurately a slope of $-4/3$ in the log–log plot. Under Θ conditions, the exponent is, in good approximation, -1. Such a good correspondence was also reported by Dan and Tirrell, who studied tethered polymers in curved geometries.[33] The central part of the profile is widest for $\chi_{BS} = 0$ (approximately 30 layers) and smallest for $\chi_{BS} = 0.5$ (only 10–15 layers). From the analysis of Wijmans and Zhulina it is expected that the central part is more important when the core is small and the grafting density high. In the present simulation of micelles the grafting density σ increases linearly with the radius R of the core ($(4\pi/3)R^3/N_A$ chains on an area $4\pi R^2$) so that

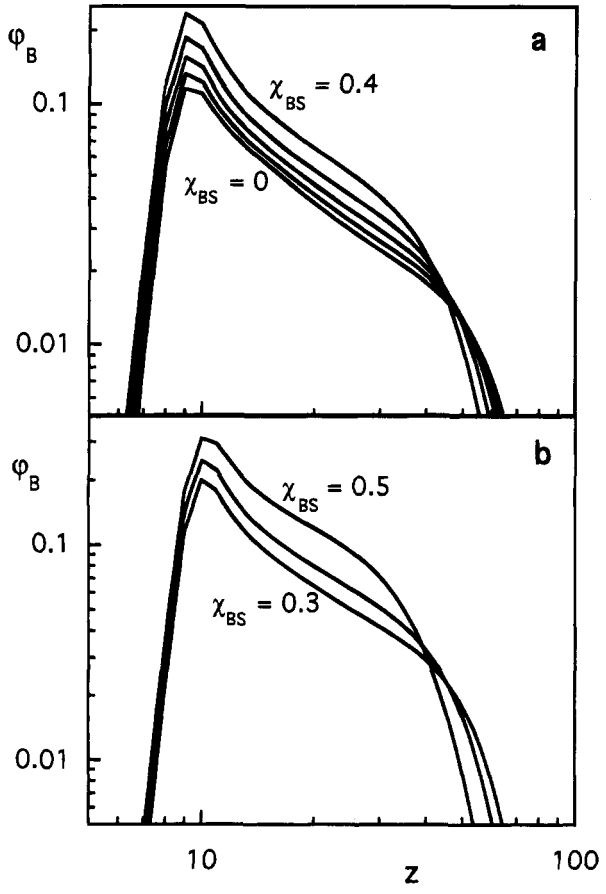

Figure 5. Radial segment volume fraction profiles for micelles with (a) $n_pN_p = 20\,000$ and (b) $n_pN_p = 28\,000$ polymer units ($N_p = 550$).

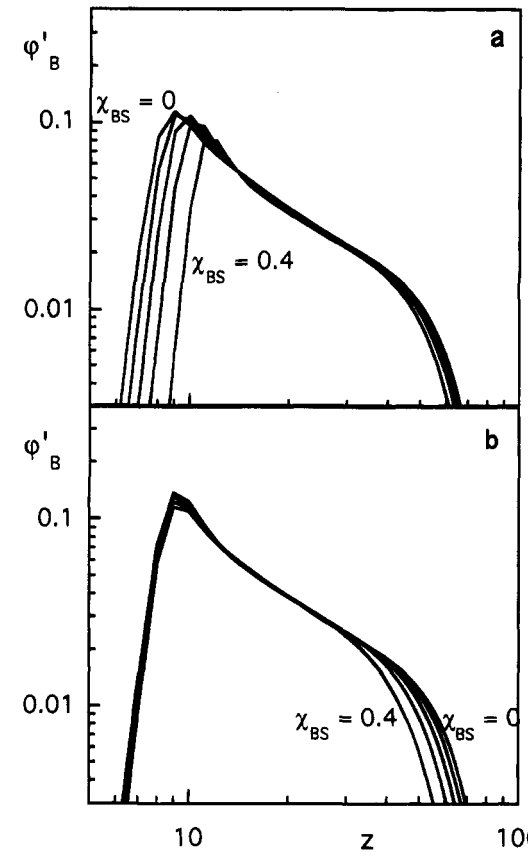

Figure 6. Testing of the scaling relation for the central part of the corona profile. In a the data of Figure 4b are replotted on modified density scales, whereas in b the data of Figure 5a are replotted. For the definitions of the normalized segment densities φ'_B, see text.

the quantities R and σ are no independent variables. If one wants to study this central part of the corona profile experimentally (which is, for example, possible using a suitable scattering technique), it is important to make a good choice for the architecture of the used copolymers. We explore the effects of a different chain composition in Figure 7.

In Figures 3d and 4d we expanded the profiles shown in Figures 3a and 4a. Where the power-law profile ends, the profile corresponding to a parabolic potential profile starts. In this part of the profile chain ends are present. As discussed by Wijmans and Zhulina the power-law part of the profile is a "dead zone" which is virtually without chain ends. In fact the dead zone comprises the central part of the profile and extends slightly in the parabolic regime. We do not illustrate the dead zone here because it has been extensively studied by others.[9,33,34] As an example, we plot the analytical profile as given in the Wijmans–Zhulina paper[9] for $\chi_{BS} = 0$ in the inset of Figure 4d. With this information it should be possible to recognize, also for the inexperienced eye, the "parabola-like" regions of the density profile. The deviations of the analytical results from the numerical ones are because in the analytical theory the chain parts that form the parabolic brush are all of equal length, which all are supposed to start at the same distance from the core. In the numerical theory the crossover from the central to the parabolic regime is not sharp, and not all chain parts in the parabolic region are equally long. This leads to a "parabolic" profile that corresponds to polydisperse grafted chains grafted onto a "rough" surface. The volume fraction profile of a polydisperse brush has been shown (on flat interfaces) to differ considerably from the homodisperse one and *may be even convex with respect to the z-axis in some extreme cases.*[35]

A fourth regime in the brush profiles can be recognized in Figures 3c and 4c. This outermost part of the profiles might be called *distal*, in analogy to the distal profile in polymer adsorption profiles.[32] Other names for this part of the profile exist. It is often referred to as the "foot" or the "tail" of the brush. It describes the approximately exponential decay of the density profile toward the polymer density in the bulk, as illustrated by the nearly linear sections in Figures 3a and 4a. Most probably, the slight deviation from an exact exponential dependence in this part of the profile is due to the curvature at the periphery of the micelle. Note that in this region the density profiles are extremely dilute so that we do not expect that this part of the profile effects the overall physical characteristics very much. Possibly the only exception is that the inner part of the distal region might influence the hydrodynamic radius of the micelles and thus could play a role in concentrated micellar solutions. The periphery of the distal profile is too dilute to be of any consequence.

As stated above, the segment density profiles of Figure 3 correspond to micelles at the CMV. For the system discussed above, the CMV is situated at a concentration well below 10^{-10}, which is too low to be measured using any available technique. Therefore, the profiles at a given micelle volume fraction, as shown in Figure 4, are probably more appropriate. We might arbitrarily use an ad hoc definition of the CMV as that composition where the micelle volume fraction becomes

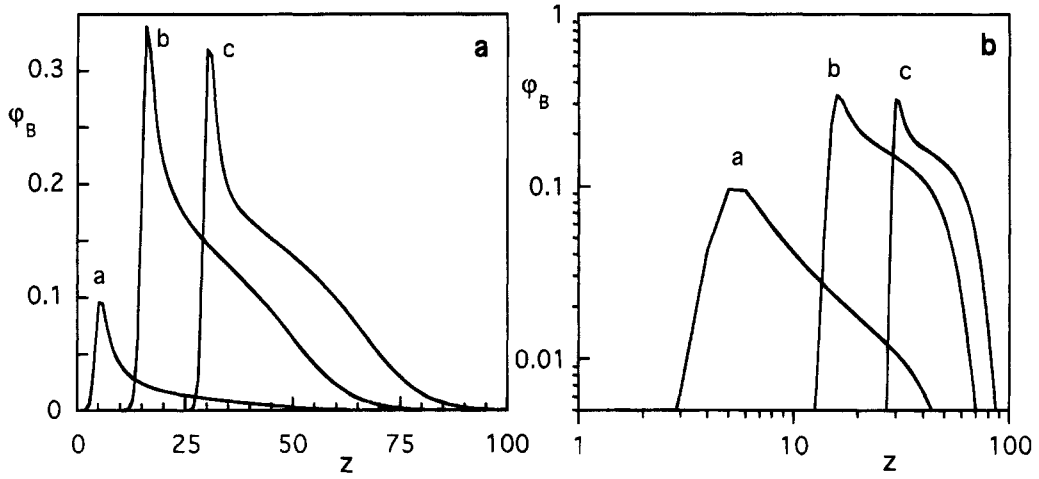

Figure 7. Radial segment distribution of the corona's of three different systems. (a) $A_{25}B_{500}$ at $\chi_{BS} = 0$, $n_p = 8.6$, $A^\sigma/k_BT = 9.6$, and $\varphi^b = 2.5 \times 10^{-4}$. (b) A micelle composed of $A_{50}B_{500}$ in the presence of A_{10} chains which partition into the micelle at $\chi_{BS} = 0$, $\varphi_{A_{10}}{}^b = 8 \times 10^{-6}$, $n_{A_{10}} = 363$, $n_p = 164$, and $A^\sigma/k_BT = 40$. (c) $A_{250}B_{500}$ at the CMV: $\chi_{BS} = 0.5$, $n_p = 367$, and $A^\sigma/k_BT = 1021.9$. In diagram a the profiles are on a linear–linear scale, whereas in diagram b a log–log scale is used.

e^{-10}. This choice corresponds to a horizontal cross section in Figure 1a. In Figure 4 the micelles have a higher aggregation number than in Figure 3. In the system with the worst solvency parameter for the B block ($\chi_{BS} = 0.5$) the aggregation number has increased most strongly. Although the number of copolymers per micelle is increased by a factor of 2 or 3 in Figure 4 compared to the micelles shown in Figure 3, the relative importance of the central regime is the same in both data sets. This is due to the fact that with increasing aggregation number (grafting density) the radius increases as well: as discussed above n_p is proportional to R.

Perhaps equally informative is the comparison of micelles at constant aggregation number, i.e., corresponding to a vertical cross section in Figure 1a. In the present set of calculations there is no given aggregation number which corresponds to an equilibrium micelle structure for all six solvency conditions. For this reason we have plotted corona profiles of micelles with a total number of polymer segments of 20 000 ($n_p \approx 36$) for $\chi_{BS} = 0$, 0.1, 0.2, 0.3, and 0.4 in Figure 5a and profiles for a segment aggregation number of 28 000 ($n_p \approx 51$) for $\chi_{BS} = 0.3$, 0.4, and 0.5 in Figure 5b. Consistent with the results shown in Figures 3 and 4, we again find the expected power-law exponents in the central part.

The scaling theory[9,34] predicts that $\varphi \propto (n_p)^{2/3}v^{-1/3}$ in the central regime for $\chi_{BS} < 0.5$ (where we defined $v = 1-2\chi_{BS}$). We therefore normalized the segment densities by those at $\chi_{BS} = 0$ by defining $\varphi'(z) \equiv f\varphi(z)$, where the proportionality constant f is given by $f = (n_{p0}/n_p)^{2/3}v^{1/3}$, where n_{p0} is defined as $n_p(\chi_{BS}=0)$. By definition, $f = 1$ for $\chi_{BS} = 0$. Applying this scaling relation to the data of Figure 4a results in a collapse of all the curves in the central part of the profile into one curve, as shown in Figure 6a. The same occurs with the data of Figure 5a, which is demonstrated in Figure 6b. This result can be considered as proof that the central part indeed shows the predicted scaling behavior. As expected, in the proximal and the parabolic regime the curves do not coincide.

From the above it is clear that our self-consistent-field theory is able to recover the predictions of the scaling analysis for the density profiles of the corona. Apparently the corona can be considered as chains "grafted" to the core. With this observation in mind we can understand the success of the SCF theory: it is known that mean-field theories essentially give a correct description for end-grafted polymers.

It is possible to vary the radius of the core R and the polymer aggregation number in micellar systems. Such variations may effect the extension of the central part of the corona profile. This is important from the point of view of, e.g., the analytical modeling of micelles. Often the free energy of the corona is computed by the blob scaling theory, with the implicit assumption that only the central regime is present in the corona. For this type of analysis it is important to know how large the central region of the profile is. We will examine three ways to reduce the importance of the central part of the profile in Figure 7.

The first method is to increase the asymmetry of the polymeric surfactants. In Figure 7 (curve a), we plot the corona profile for micelles composed of $A_{25}B_{500}$ molecules, under good solvency conditions for the B segments ($\chi_{BS} = 0$). In this case the CMV reaches measurable values (CMV $\approx 2 \times 10^{-4}$) and the aggregation number is low. In this case, the micelle is too small to cause a wide power-law region. The power-law regime is found only between layers 7 and 12 (see Figure 7b).

The second way to trim the power-law character of the profile is presented in curve b of Figure 7. In this example we have added a compound which solubilizes into the micelle, so that the core swells and thereby becomes less strongly curved than in our reference system. This type of system has recently been addressed by several authors.[14-16,36] As an example we choose A_{10} molecules. The bulk concentration of the A_{10} molecules is slightly below the saturation value for these molecules in the solvent. As can be noticed in Figure 7, the central part has vanished completely for this case.

A third way to suppress the central part in the corona profile is shown in curve c of Figure 7. The polymeric surfactant is now a rather symmetric block copolymer $A_{250}B_{500}$, for which the B block is in Θ conditions ($\chi_{BS} = 0.5$). The micelles formed by these surfactants have a large core block which results in an extremely low CMV and a large aggregation number. In Figure 7 we show the profile of the smallest micelle of this type that is stable (i.e., at the CMV). Compared to our reference $A_{50}B_{500}$, the core of the micelles has grown so much that the curvature in the brush layer is too small to sustain a noticeable central part in the brush profile. A conclu-

sion from parts a and b of Figure 7 is that it is possible that the proximal and the parabolic profiles can cross over smoothly, bypassing the central region of the profile completely.

The profiles discussed above could in principle be measured experimentally, e.g., by neutron scattering or small-angle X-ray scattering techniques. In such experiments one could try to search for a central part in the corona profile. It should be realized, however, that the relative importance of the central part is not always large. In many practical polymer surfactant systems the central part could even be virtually absent. Well-chosen polymeric surfactants should, however, show a central part in the corona profile, which is not lost when the micelle size and micelle concentration are varied, although the relative importance of the central regime is still a function of the aggregation number (core size).

Conclusions

We have shown that polymeric micelles have very interesting segment density profiles. In particular, the corona of the micelles can, when the molecular conditions are chosen carefully, consist of four consecutive regimes. Starting at the core–corona boundary and moving outward, we may distinguish (1) a proximal regime where adsorption processes are important, (2) a central regime which follows the predicted power-law behavior both in Θ and in good solvents, (3) a parabola-like profile which corresponds to a parabolic potential profile, and (4) the distal regime where the density profile falls off exponentially to the bulk value. The relative importance of the central part of the corona profiles is strongly affected by the chain composition and, indirectly, by the core size.

In many cases the real CMV in polymeric systems is too low to be measured experimentally. Any measurable micelle is often larger than a micelle at the CMV. The aggregation number remains relatively low only for molecules with rather asymmetric architecture.

The SCF model used in this study can be routinely applied for the modeling of copolymer self-assembly phenomena. The model is not restricted in the architecture of the copolymers. Furthermore, it is possible to extend the model to multicomponent systems and systems with long-range electrostatic interactions.[37]

References and Notes

(1) Marques, C.; Joanny, J.-F.; Leibler, L. *Macromolecules* **1988**, *21*, 1051.
(2) Linse, P. *Macromolecules* **1994**, *27*, 6404.
(3) Leibler, L.; Orland, H.; Wheeler, J. C. *J. Chem. Phys.* **1983**, *16*, 1443.
(4) Noolandi, J.; Hong, K. M. *Macromolecules* **1983**, *16*, 1443.
(5) Nagarajan, R.; Ganesh, K. *J. Chem. Phys.* **1989**, *90*, 5843.
(6) Semenov, A. N. *Sov. Phys. JETP* **1985**, *61*, 733.
(7) Milner, S. T.; Witten, T. A.; Cates, M. E. *Macromolecules* **1988**, *21*, 2610.
(8) Zhulina, E. B.; Borisov, O. V.; Priamitsyn, V. A. *J. Colloid Interface Sci.* **1990**, *137*, 495.
(9) Wijmans, C. M.; Zhulina, E. B. *Macromolecules* **1993**, *26*, 7214.
(10) Daoud, M.; Cotton, J. P. *J. Phys. (Paris)* **1982**, *43*, 531.
(11) Milner, S. T.; Witten, T. A. *J. Phys. (Fr.)* **1988**, *49*, 1951.
(12) Murat, M.; Grest, G. S. *Macromolecules* **1991**, *24*, 704.
(13) Halperin, A. *Macromolecules* **1987**, *20*, 2943.
(14) Cogan, K. A.; Leermakers, F. A. M.; Gast, A. P. *Langmuir* **1992**, *8*, 429–436.
(15) Hurter, P. N.; Scheutjens, J. M. H. M.; Hatton, T. A. *Macromolecules* **1993**, *26*, 5030.
(16) Hurter, P. N.; Scheutjens, J. M. H. M.; Hatton, T. A. *Macromolecules* **1993**, *26*, 5592.
(17) Hall, D. G.; Pethica, B. A. In *Nonionic Surfactants*; Schick, M. J., Ed.; Marcel Dekker: New York, 1976.
(18) Scheutjens, J. M. H. M.; Fleer, G. J. *J. Phys. Chem.* **1979**, *83*, 1619–1635.
(19) Scheutjens, J. M. H. M.; Fleer, G. J. *J. Phys. Chem.* **1980**, *84*, 178–190.
(20) Scheutjens, J. M. H. M.; Fleer, G. J. *Macromolecules* **1985**, *18*, 1882.
(21) Fleer, G. J.; Scheutjens, J. M. H. M.; Cohen Stuart, M. A.; Cosgrove, T.; Vincent, B. *Polymers at Interfaces*; Elsevier: London, 1993.
(22) Leermakers, F. A. M.; Scheutjens, J. M. H. M. *J. Chem. Phys.* **1988**, *89*, 3264–3274.
(23) Leermakers, F. A. M.; Scheutjens, J. M. H. M. *J. Chem. Phys.* **1989**, *93*, 7417–7426.
(24) Leermakers, F. A. M.; Scheutjens, J. M. H. M. *J. Chem. Phys.* **1988**, *89*, 6912–6924.
(25) Leermakers, F. A. M.; Scheutjens, J. M. H. M. *J. Colloid Interface Sci.* **1990**, *136*, 231–241.
(26) Leermakers, F. A. M.; van der Schoot, P. P. A. M.; Scheutjens, J. M. H. M.; Lyklema, J. In *Surfactants in Solution*; Mittal, K. L., Ed.; Plenum: New York, 1990; Vol. 7, pp 43–60.
(27) Leermakers, F. A. M.; Lyklema, J. *Colloids Surf.* **1992**, *67*, 239–255.
(28) Van Lent, B.; Scheutjens, J. M. H. M. *Macromolecules* **1989**, *22*, 1931–1937.
(29) Linse, P.; Björling, M. *Macromolecules* **1991**, *24*, 6700.
(30) Corkill, J. M.; Goodman, J. F.; Harrold, S. P. *Trans. Faraday Soc.* **1964**, *60*, 202.
(31) Evers, O. A.; Scheutjens, J. M. H. M.; Fleer, G. J. *Macromolecules* **1990**, *23*, 5221.
(32) de Gennes, P.-G. *Macromolecules* **1981**, *14*, 1637.
(33) Dan, N.; Tirrell, M. *Macromolecules* **1992**, *25*, 2890.
(34) Zhulina, E. B.; Borisov, O. V.; Priamitsyn, V. A.; Birshtein, T. M. *Macromolecules* **1991**, *24*, 140.
(35) Milner, S. T.; Witten, T. A.; Cates, M. E. *Macromolecules* **1989**, *22*, 853.
(36) Nagarajan, R.; Garnesh, K. *Macromolecules* **1989**, *22*, 4312.
(37) Israëls, R.; Scheutjens, J. M. H. M.; Fleer, G. J. *Macromolecules* **1993**, *26*, 5405–5413.

MA9460549